Journal of Alloys and Compounds 509 (2011) 8812–8824

Contents lists available at ScienceDirect

Journal of Alloys and Compounds

journal homepage: www.elsevier.com/locate/jallcom

Behavior of oxygen diffusion in buffer layers for coated conductors

Y. Wang[a,b], L. Zhou[a,b], Y.F. Lu[b,*], C.S. Li[b], Z.M. Yu[b], L.H. Jin[b], J.S. Li[a]

[a] State Key Laboratory of Solidification Processing, Northwestern Polytechnical University, Xi'an 710072, China
[b] Northwest Institute for Nonferrous Metal Research, Xi'an 710016, China

ARTICLE INFO

Article history:
Received 10 October 2010
Received in revised form 14 June 2011
Accepted 16 June 2011
Available online 30 June 2011

Keywords:
Coated conductor
Buffer layer
Metal organic deposition
Oxygen diffusion

ABSTRACT

We have evaluated the effect of annealing in oxygen atmosphere on the structure, texture and phase transformation of LZO films deposited on YSZ (yttria-stabilized zirconia) (0 0 *l*) single crystal substrates and textured NiW substrates by metal-organic deposition (MOD) method. The results show that the structure stability of the LZO films is heavily dependent on the oxygen partial pressure in annealing process. Then we have in details studied the behavior of oxygen diffusion in three kinds of buffer layer architectures on NiW substrates by varying the temperature, oxygen partial pressure and dwelling time in the annealing process. The oxygen diffusion within buffer layers leads to the oxidation of substrate, and even the texture and structure of buffer layers are destroyed with the increase of the thickness of the oxides layer related to NiW substrate. It reveals that the relative volume of oxides related to NiW substrate increases exponentially with the annealing temperature, and increases linearly with the annealing time at logarithmic scale. The relative intensity of texture peaks of buffer layers decreases and even disappears with the increase of the oxygen partial pressure in annealing process because of the acceleration of the oxidation reaction of substrate. The influence of annealing temperature, oxygen partial pressure and dwelling time on the oxygen diffusion is related to the intrinsic oxygen diffusion coefficient of buffer layers materials. Compared with the increase of oxygen partial pressure, the elongation of dwelling time shows a less effect on the oxidation rate of NiW substrate and a weak destruction of the texture of buffer layers. Except choosing the oxide materials with small oxygen diffusion coefficient as buffer layers in coated conductors, the degree of oxidation about NiW substrate could be greatly controlled and it would result in the less destruction of texture and structure of buffer layers by adjusting the annealing temperature, oxygen partial pressure and dwelling time in the process of YBCO deposition.

1. Introduction

In recent years, the second generation high-temperature superconducting coated conductors, consisting of an epitaxial superconducting layer deposited on biaxially textured flexible substrate of a metallic template with buffer layers, become the significant materials that is possible for engineering application in magnetic field and the theoretical values as well [1–4]. There exist large crystalline lattice mismatch (about 8%) and serious atom diffusion between the NiW substrate and the superconducting layer, and therefore the buffer layer, which transfers the biaxial texture in the metal substrate to the superconducting layer and simultaneously prevents the oxygen diffusion down to the substrate, as well as prevents the diffusion of metal atoms up into the superconducting layer, is the multi-functional layer in the structure of coated conductors. High temperature and oxidation atmosphere are generally adopted to obtain the superconducting phase and also to increase superconducting current carrying capacity of coated conductors. But in this process, oxygen atoms may diffuse through the buffer layer down to the substrate to cause oxidation of the metal, so the biaxial texture of the buffer layer and superconducting layer would be destroyed. Therefore, the study about the behavior of oxygen diffusion in buffer layer is significant to the development and application of coated conductors, especially for the selection of buffer layer materials and the optimization for preparation techniques of superconducting layer.

Metal organic deposition (MOD) has emerged as a highly attractive choice to prepare oxide films in terms of low-cost and non-vacuum process compared with physical vapor deposition (PVD) [5,6]. The procedures, which $La_2Zr_2O_7$ (LZO) and CeO_2 textured thin films are prepared on YSZ (yttria-stabilized zirconia) (0 0 *l*) single crystal substrates and textured NiW substrates by MOD, are well controllable and rather mature [7–15]. In addition, there exists large difference between the intrinsic oxygen diffusion coefficient of LZO and that of CeO_2 [13,16]. Hence, we prepared 70 nm thick LZO films with a pyrochlore structure on YSZ (0 0 *l*) single crystal substrates (LZO/YSZ) and on textured NiW substrates (LZO/NiW) in Ar–4%H_2 by MOD method. The textured LZO films

* Corresponding author. Tel.: +86 29 86231079; fax: +86 29 86224487.
E-mail address: wyspacestar@yahoo.com.cn (Y.F. Lu).

0925-8388/$ – see front matter © 2011 Elsevier B.V. All rights reserved.
doi:10.1016/j.jallcom.2011.06.081

on YSZ (0 0 l) single crystal substrates and textured NiW substrates are then annealed in oxidation atmosphere with a larger range of oxygen partial pressure. Our results show that annealing in oxygen has significant effect on microstructure and texture transformation performance of LZO film. Then three kinds of 70 nm thick buffer layer architectures, including single LZO layer, single CeO_2 layer, LZO and CeO_2 double layers on NiW substrates (LZO/NiW, CeO_2/NiW, CeO_2/LZO/NiW) separately, are selected as model system to carry out the research about the behavior of oxygen diffusion in buffer layers for coated conductors. The choice of 70 nm thickness for these buffer layer architectures lies on the fact that more than 80 nm of LZO is thick enough to ensure a good barrier against nickel and oxygen diffusion in the growth process of superconducting layer [13]. These textured buffer layers fabricated firstly respectively in Ar–4%H_2 by MOD method are annealed again at different temperatures in oxidization atmosphere with different oxygen partial pressures for different dwelling time. The thermodynamics and kinetics processes of oxygen diffusion in buffer layer for coated conductors are explored elementarily by investigating the change of their structure, texture and morphology among as-grown and annealed samples in different conditions.

2. Experiment

All buffer layers with the same thickness were prepared on YSZ (0 0 l) single crystal substrates and textured NiW substrates in Ar–4%H_2 by MOD method. The starting solution for LZO was prepared by mixing a stoichiometric amount of reagents lanthanum (III) 2, 4-pentanedionate and zirconium (IV) 2, 4-pentanedionate (received from Strem) with propionic acid. After heated at 75 °C for 25 min with continuous stirring, a stable yellow-colored LZO solution was obtained. Similarly cerium (III) 2,4-pentanedionate (received from Strem) was dissolved in propionic acid by heating with continuous stirring to obtain a stable brown-colored CeO_2 precursor solution. All precursor solution manipulations were carried out in ambient atmosphere. Details of their preparation processes can be found elsewhere [7–14]. The LZO precursor solution was firstly spin coated onto YSZ (0 0 l) single crystal substrates and short cube-textured NiW substrates of 1 cm × 1 cm in size at 2500 rpm for 30 s; followed by heat treatment at 900 °C for 1 h in a reducing forming gas atmosphere of Ar–4% H_2. After crystallized, these samples were annealed at 900 °C for 1 h in oxidation atmosphere with a large range of oxygen partial pressure to study the effect of annealing in oxygen on the structural stability of LZO films.

In addition, the LZO and CeO_2 precursor solutions were spin coated onto short cube-textured NiW substrates of 1 cm × 1 cm in size at 2500 rpm for 30 s; followed by heat treatment at 900 °C for 1 h in a reducing forming gas atmosphere of Ar–4% H_2. At the end of the heat-treatment cycles, the samples were quenched to room temperature in the same atmosphere to obtain the single LZO and CeO_2 buffer layers, respectively. The each LZO and CeO_2 precursor solution for the CeO_2/LZO double layers was obtained by diluting their above as-prepared solutions through adding propionic acid. Likewise, spin coating was used to deposit LZO films firstly at a spin rate of 2500 rpm for 30 s onto NiW substrates. Then the LZO coatings were annealed at 900 °C for 1 h in a flowing gas (Ar–4%H_2) atmosphere. Afterwards, the procedures were repeated using the CeO_2 solution to prepare the textured CeO_2/LZO double layers. Subsequently, these as-prepared textured buffer layers were annealed at different temperatures in oxidization atmosphere with different oxygen partial pressures for different dwelling time to investigate their thermodynamics and kinetics processes of oxygen diffusion.

The as-grown single LZO layer, single CeO_2 layer and CeO_2/LZO double layers and annealed samples at different conditions, respectively, were characterized by using X-ray diffraction (XRD), which was performed to carry out $\theta - 2\theta$ scan by using CuKα radiation at 40 kV and 50 mA, for phase purity and texture. The thicknesses of all buffer layers prepared under the same conditions were calibrated by using an-step apparatus. High temperature in situ XRD experiments were carried out in ambient atmosphere and heating ramp of 10 °C min^{-1} for nucleation and growth of oxides related to NiW substrate. The lattice parameters were determined from XRD patterns using the MDI-JADE-6 program. The homogeneity and microstructure analysis of these samples were performed by using JSM-6700 field emission scanning electron microscopy (SEM) equipped with Energy Dispersive Spectrometry (EDS) and a digital instruments nanoscope SPI3800-SPA-400 atomic force microscopy (AFM) in contact mode.

3. Results and discussion

The buffer layers in coated conductors are usually deposited in the reducing atmosphere to avoiding the surface oxidation of metal substrates, especially for CSD route. Therefore, a relatively large number of lattice oxygen vacancies would form in oxide crystal structure. However, when the crystallized oxide films are annealed in oxidization atmosphere, their structural stability would be seriously challenged due to the possible diffusion of oxygen atoms and the lowered density of the lattice oxygen vacancies. The optimal oxygen partial pressure is 0.1% during preparation of superconducting layers in coated conductors [17–19], so we select the oxidation atmosphere with the oxygen partial pressure from 0.5% to 100%, in which LZO films on YSZ (0 0 l) single crystal substrate and NiW substrate are annealed. The effect of annealing in oxygen on the structure and texture of LZO films is investigated.

XRD patterns, which are obtained for as-grown LZO films on YSZ (0 0 l) single crystal substrates prepared at 900 °C for 1 h in Ar–4%H_2 and annealed samples at 900 °C for 1 h in oxidation atmospheres, are illustrated in Fig. 1(a). The LZO films prepared at 900 °C for 1 h in Ar–4%H_2 have completely crystallized to form a preferred orientation along the (0 0 l) direction. Moreover, the sharp LZO (0 0 l) diffraction peak can still be observed for all samples after annealed at 900 °C for 1 h in Ar–0.5% O_2, Ar–10% O_2 and pure oxygen, respectively. It indicates that the (0 0 l) orientation of LZO crystallized films on YSZ (0 0 l) single crystal substrates does not be destroyed after annealing in oxidation atmospheres. Fig. 1(b) plots the FWHM of (2 2 2) phi-scans for LZO films on YSZ (0 0 l) single crystal sub-

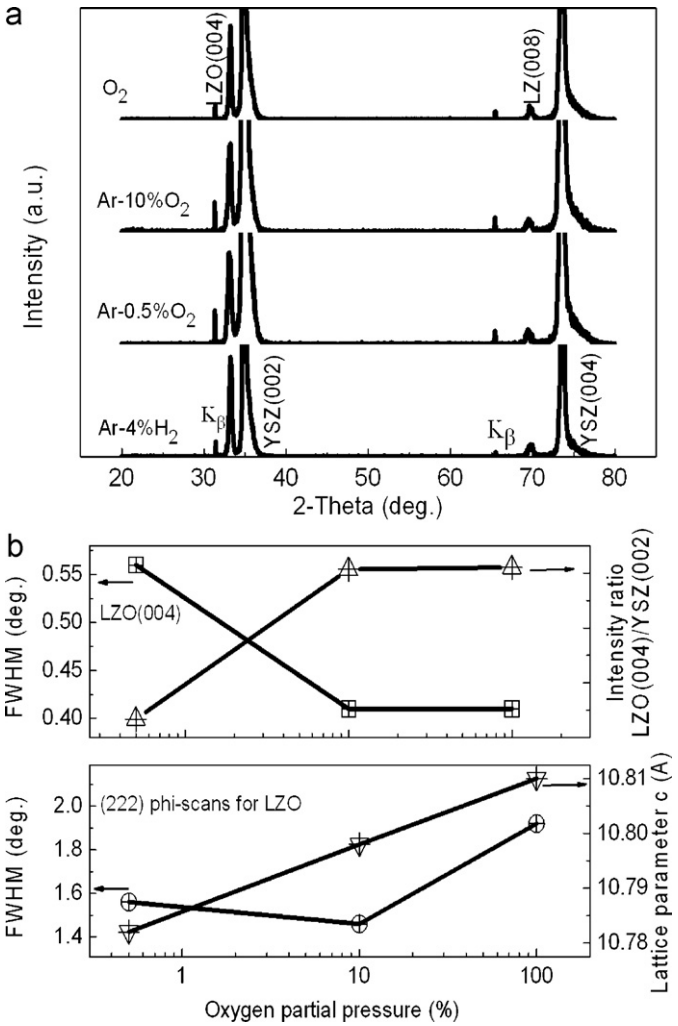

Fig. 1. (a) XRD patterns for the as-grown and annealed LZO/YSZ samples in Ar–0.5% O_2, Ar–10% O_2 and O_2; (b) dependence of the FWHM of (2 2 2) phi-scans of LZO films, the lattice parameter, FWHM of LZO (0 0 4) diffraction peaks and the relative intensity (determined by taking the intensity ratio of the LZO (0 0 4) to the YSZ (0 0 2) X-ray diffraction peaks) on the oxygen partial pressure in annealing atmosphere.

strates, the lattice parameter of LZO, the FWHM values for LZO (0 0 4) peaks, as well as the intensity ratio of LZO (0 0 4) to the YSZ (0 0 2) diffraction peaks, which gives an estimate of the amount of orientation crystalline fraction in the films, as a function of the oxygen partial pressure in annealing atmosphere. The oxygen partial pressure has not an apparent effect on the in-plane texture of LZO films on YSZ (0 0 *l*) single crystal substrates, as evidenced by the little change in the phi-scans FWHM compared with that of the as-grown samples. It indicates that the annealing in oxygen cannot improve or destroy the texture of LZO films on YSZ substrates. However, the shift of the LZO (0 0 4) peak positions toward lower diffraction angles indicates a gradual increment in the lattice parameter *c* with the increase of the oxygen partial pressure in annealing atmosphere, as seen in Fig. 1(b). It can be explained by the decrease of the number of lattice oxygen vacancies in LZO pyrochlore structure during annealing in oxidation atmosphere. It can be clearly seen that the FWHM value for LZO (0 0 4) primarily decreases and then remains almost invariable, on the contrary, the intensity ratio of LZO (0 0 4) initially increases and afterwards keeps unaltered with the increase of the oxygen partial pressure in annealing atmosphere. We speculate that increasing the oxygen partial pressure up to, but not exceeding, 10% during annealing processes may enhance the crystalline in the LZO films on YSZ (0 0 *l*) single crystal substrates by incorporation more oxygen into the lattice vacancies. And this trend becomes inconspicuous when the volume percentage of oxygen is beyond 10% in annealing atmosphere. In other words, the crystalline degree of LZO film increases speedily and reaches a maximum for the optimally oxidized sample annealed in Ar–10%O_2. It might be responsible for almost saturated supply of oxygen atoms to lattice oxygen vacancies in LZO film when the volume of oxygen in annealing atmosphere reaches 10%.

The typical XRD $\theta - 2\theta$ scan results of the as-grown LZO films on NiW substrates obtained at 900 °C for 1 h in Ar–4%H_2 and annealed samples in oxidation atmospheres are shown in Fig. 2(a). The LZO films prepared at 900 °C for 1 h in Ar–4%H_2 have completely crystallized to form the preferred orientation along the (0 0 *l*) direction. But for each samples after annealing in Ar–0.5% O_2, Ar–10% O_2 and pure oxygen, the obvious diffraction peaks of some oxides related to Ni and W including $NiWO_4$ and NiO, are observed besides the weakened LZO (0 0 *l*) peak. It indicates that the destruction of (0 0 *l*) orientation LZO film is not beneficial to the transfer of the biaxial texture of NiW substrate to the superconducting layer after annealing in oxidization atmosphere because of the oxidation of NiW substrates. It means that about 70 nm thick LZO films are not able to effectively prevent diffusion of oxygen into NiW substrates during 900 °C high-temperature processing even in a low oxygen partial pressure [15]. Furthermore, during annealing in oxidation atmosphere, it is highly possible that the nucleation of oxides related to Ni and W occurs first at the interface between LZO layer and NiW substrate and the growth front develops from the interface between LZO layer and NiW substrate to the surface of buffer layer. During the annealing process in oxidation atmosphere, if a large amount of these oxides diffuse into the LZO layer and disturb the LZO crystal structure, the LZO film may loss its (0 0 *l*) texture, which will lead to the failure of the biaxial texture transfer in coated conductors. Fig. 2(b) illustrates the intensity ratio of these oxides phases, which is estimated by dividing the intensity of the NiW (0 0 2) X-ray diffraction peak by the sum of intensities of $NiWO_4$ and NiO polycrystalline phases in the films, as a function of the oxygen partial pressure in annealing atmosphere. It shows that the $NiWO_4$ is the main phase on the surface of the sample annealed in Ar–0.5%O_2. As the oxygen volume percentage increases to above 10%, the NiO becomes the main phase. The amount change of the $NiWO_4$ and NiO phases dependent on the oxygen partial pressure suggests that the activation energy of these oxides formation is related to

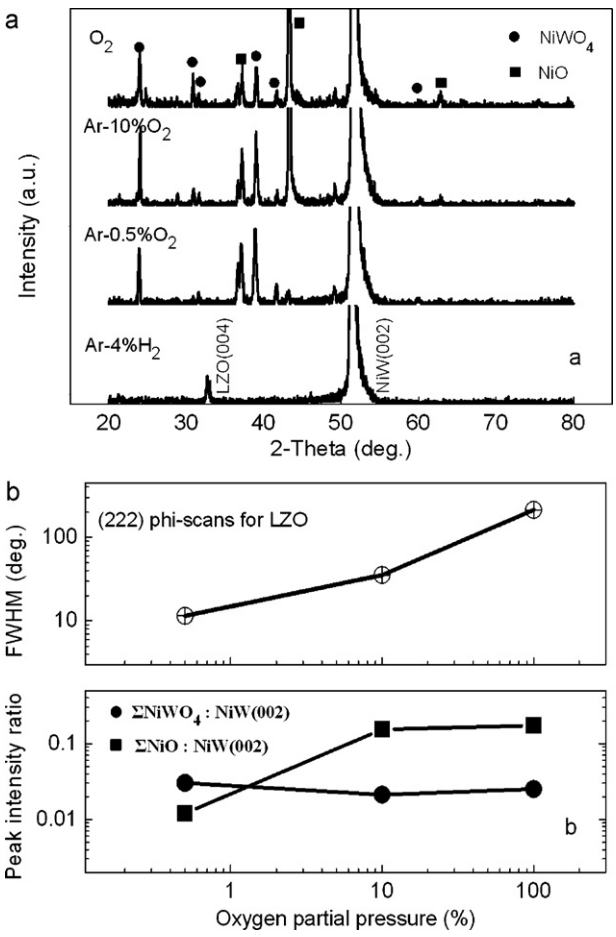

Fig. 2. (a) $\theta - 2\theta$ scans of the as-grown and annealed LZO/NiW samples in Ar–0.5% O_2, Ar–10% O_2 and O_2; (b) variation of the intensity ratio of the oxides related to NiW substrates (determined by dividing the intensity of NiW (0 0 2) X-ray diffraction peaks by the sum of intensities about all oxide phases) and the FWHM of (2 2 2) phi-scans of LZO films in different annealing atmosphere.

the annealing condition. For the NiO phase, the increase of oxygen partial pressure is in favor of the decrease of its activation energy, on the contrary, there is less influence on the activation energy of $NiWO_4$, of which little decomposition even occurs at the higher oxygen partial pressure. In fact, for the RABiTS route, the formation of $NiWO_4$ in buffer layers/metal substrate during the preparation of superconducting layers is easily found in other architectural coated conductors, if the functional layers undergo annealing in oxygenation atmosphere for a relatively long time [20,21]. However, the nucleation and growth of the NiO phase need much more driving energy than that of the $NiWO_4$. In any case, the formation of the $NiWO_4$ and NiO oxides is so quick as to ultimately destroy the structure of the LZO films under the influence of heating and oxygen. Fig. 2(b) plots the FWHM of (2 2 2) phi-scans for LZO films on NiW substrates, annealed at 900 °C as a function of the oxygen partial pressure in annealing atmosphere. It is found that annealing in oxidation atmosphere has a significant negative affect on the in-plane texture of LZO films on NiW substrates, as proofed by the substantial increase in the phi-scans FWHM. It may be because NiO and $NiWO_4$ formed in the annealing process diffuse into LZO layer and disturb the LZO crystal structure, which leads to the decrease of texture degree for LZO films on NiW substrates. The sign of the existence of these oxides related to Ni and W is from the $\theta - 2\theta$ spectrum.

A single MOD-LZO buffer layer is sufficient to ensure structural compatibility between YBCO and NiW, so its main function

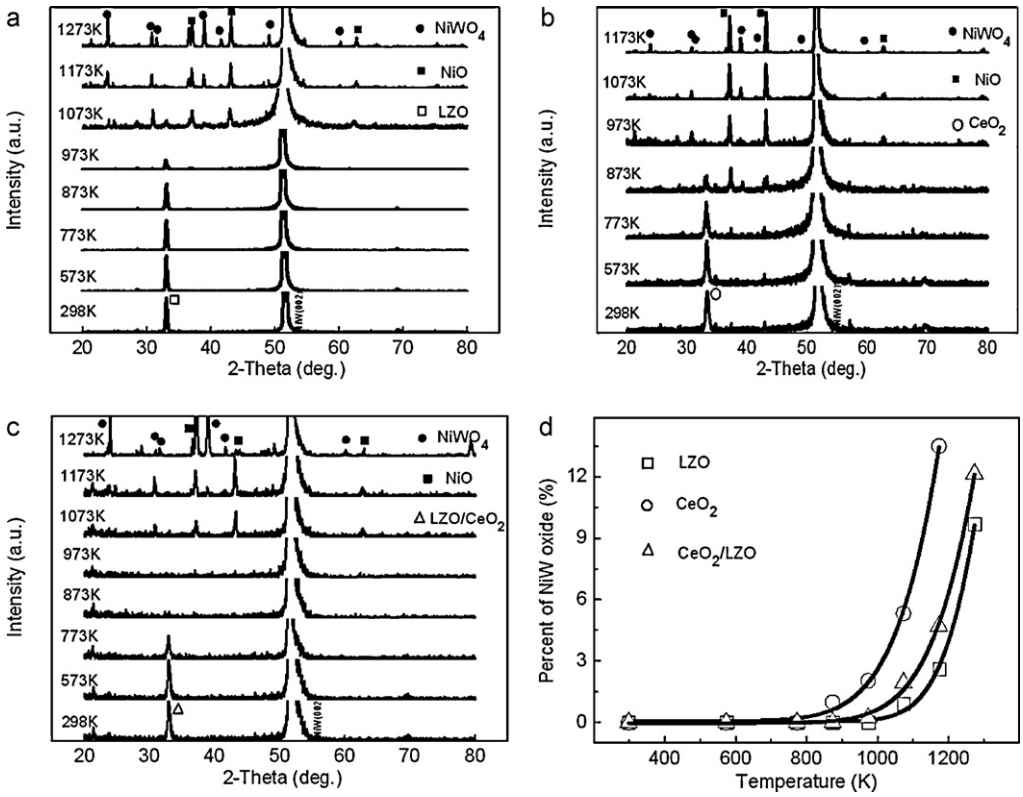

Fig. 3. The high temperature in situ XRD spectrums for as-grown and annealed (a) LZO/NiW, (b) CeO_2/NiW and (c) CeO_2/LZO/NiW samples at various temperatures ranging from 300 °C to 1000 °C, respectively; (d) the percentage of NiW oxides in three kinds of samples at different annealing temperature.

should include transferring the biaxial texture from NiW substrate to YBCO layer and protecting the substance from oxidation during heat-treatment process. According to the recent reports [13,22], the single LZO layer with a thickness more than 80 nm is thick enough to ensure a good barrier against nickel and oxygen diffusion during preparation of the superconducting layer. For the 70-nm thickness single LZO layer, its lower 30 nm is disturbed due to the oxidation of substrate, but its top 30 nm remains good biaxial texture after YBCO deposition. And on NiW substrate, $NiWO_4$, NiO and LZO layers are detected in sequence [15]. Here 70 nm thick LZO films with good biaxial texture are obtained by MOD, but $NiWO_4$ and NiO phases are detected on the surface of the samples after annealing in oxidation atmosphere. It means that the ability to preventing oxygen diffusion in these LZO films is very limited and the oxide films related to Ni and W are so thick that the texture and surface morphology of LZO films are destroyed entirely in our case with relatively high oxygen partial pressure.

Here the thermodynamics and kinetics of oxygen diffusion in buffer layer for coated conductors could be explored by investigating the relationship between the change of texture and microstructure for buffer layers and the formation of oxides phases about NiW substrate by varying temperature, oxygen partial pressure and dwelling time in the annealing process.

We firstly investigate the effect of annealing temperature on oxygen diffusion through three kinds of buffer layer architectures in the oxidation atmosphere with high oxygen partial pressure and then analyze thermodynamics of oxygen diffusion. Fig. 3(a)–(c) shows the high temperature in situ XRD spectrums for the crystallized LZO/NiW, CeO_2/NiW and CeO_2/LZO/NiW samples annealed at various temperatures ranging from 300 °C to 1000 °C for a fixed dwelling time of 10 min in ambient atmosphere, respectively. For the buffer layers crystallized in Ar–4%H_2, the sharp (0 0 l) reflections of are observed, indicating the well-orientated films of LZO, CeO_2 and LZO/CeO_2 on NiW. With the increase of the annealing temperature in ambient atmosphere, however, $NiWO_4$ and NiO polycrystalline phases appear accompanied with the decrease and even disappearance of (0 0 l) reflections of the buffer layers in the samples, suggesting that the orientation of these buffer layers is gradually destroyed due to the oxidation of NiW substrates. But it should be pointed out that the annealing temperature, at which the oxides phases related to NiW substrate begin to be detected in LZO/NiW, is the highest, while it is the lowest in CeO_2/NiW. Moreover, the amount of NiO phase in LZO/NiW is less than that in CeO_2/NiW at the same annealing temperature. It indicates that LZO is a better barrier against oxygen diffusion than CeO_2 as buffer layer in coated conductors. Fig. 3(d) gives the experimental result and the theoretical fit of the percentage of NiW oxides as annealing temperature, where the percentage of oxides related to NiW (wt%) is defined as a ratio of $(I_{NiWO_4} + I_{NiO})/(I_{NiW} + I_{NiWO_4} + I_{NiO})$ obtained through dividing the sum of intensities of NiW (0 0 2) diffraction peak (I_{NiW}), $NiWO_4$ (I_{NiWO_4}) and NiO (I_{NiO}) polycrystalline phases by the sum of I_{NiWO_4} and I_{NiO}. The curves show an exponential increase with the annealing temperature, which may be related with the speedup of oxygen diffusion and oxidation reaction of NiW substrate when the annealing temperature rises. The temperature, at which the oxidation products of NiW begin to be detected and meanwhile the (0 0 l) textured peaks of the buffer layers disappear, varies for LZO/NiW, CeO_2/NiW and CeO_2/LZO/NiW, for example, 750 °C, 550 °C and 700 °C, respectively. This temperature is here denoted as so-called critical temperature of T^*. The thermodynamics of these oxidation processes can be described by Arrhenius equation, as below

$$k = A \exp\left(\frac{-E_\alpha}{RT}\right) \quad (1)$$

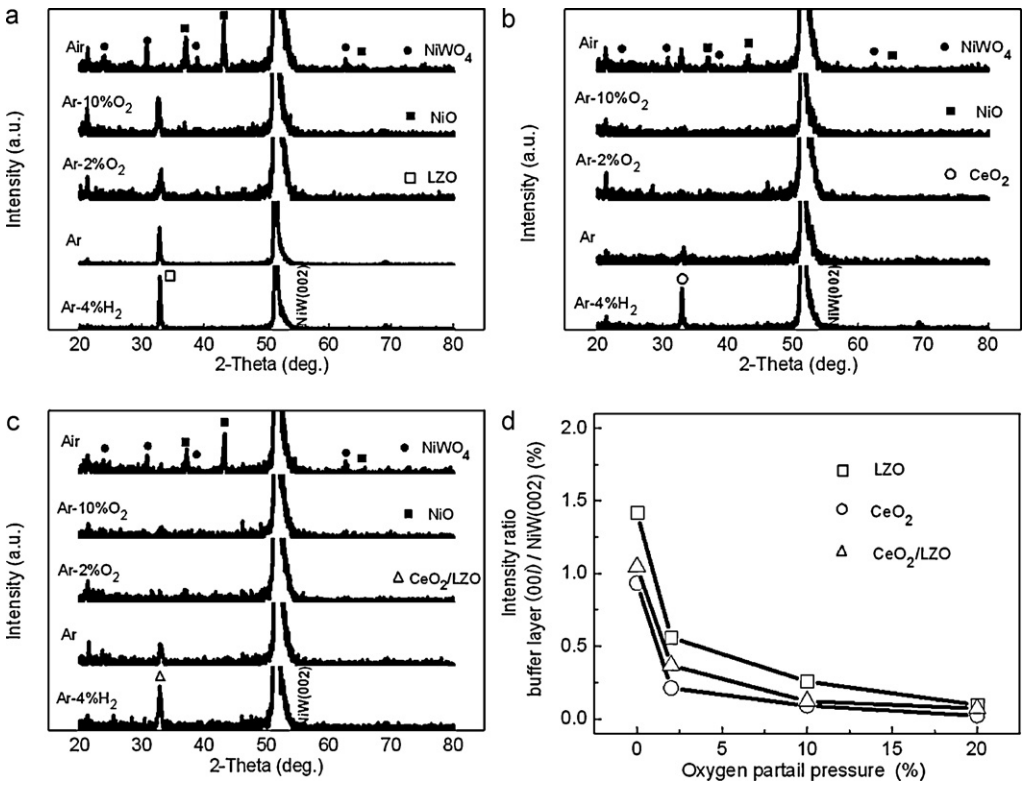

Fig. 4. XRD patterns of as-grown and annealed (a) LZO/NiW, (b) CeO_2/NiW and (c) CeO_2/LZO/NiW samples in oxidation atmosphere with different oxygen partial pressure, respectively; (d) dependency of the intensity ratio (computed through dividing the intensity of buffer layers (0 0 *l*) peaks by that of NiW (0 0 2)) in three kinds of samples on oxygen partial pressure in annealing process.

where k is the reaction rate coefficient, A denotes the frequency factor of the oxidation reaction of NiW substrate assumed to be a constant in the same buffer layer architecture, E_a is the activation energy, the universal gas constant R has the value of 8.314 J mol^{-1} K^{-1} and T is the heat-treatment temperature. Because the thickness of as-prepared buffer layers is only about 70 nm and the oxygen partial pressure adopted in annealing process is as high as 20%, the concentration gradient of oxygen atoms in the buffer layer is assumed to be negligible. Therefore, we believe that k is proportional to the percentage of NiW oxides for the same dwelling time in annealing process. This is given by expression (2):

$$k \propto \text{wt\%} \tag{2}$$

According to Eq. (1) and expression (2), it is derived as below:

$$\text{wt\%} \propto A \quad \exp\left(\frac{-E_\alpha}{RT}\right) \tag{3}$$

With the help of Eq. (3) in combination with the experimental data from Fig. 3(d) the E_a values of the oxidation reactions of NiW substrate are 163.48 kJ mol^{-1}, 89.88 kJ mol^{-1} and 113.27 kJ mol^{-1} in LZO/NiW, CeO_2/NiW and CeO_2/LZO/NiW samples, respectively. The nucleation process of oxides related to NiW substrate is controlled by the activation energy [23]. A greater E_a generally indicates a slower reaction rate. The experimental results are just consistent with this law, illuminating that the oxidation of NiW substrate is the most difficult in LZO/NiW, while in CeO_2/NiW it becomes the easiest among the above-mentioned samples. On the other hand, the intrinsic oxygen diffusion coefficient of each buffer layers is very different. For the buffer layers with the same thickness, it can be speculated that the activation energy of the oxidation reaction about NiW could decrease with the increase of oxygen diffusion coefficient for the buffer layer. It indicates that the intrinsic oxygen diffusion coefficient of the buffer layer is relevant to the oxidation procedure of NiW substrate in each sample during the annealing process in oxidation atmosphere.

Now we study the dependence of oxidation reaction about NiW substrate on oxygen partial pressure in above-mentioned samples with three different buffer layer architectures at their critical temperature for the same dwelling time of 10 min during annealing process. Fig. 4(a)–(c) shows the XRD $\theta-2\theta$ patterns of the LZO/NiW, CeO_2/NiW and CeO_2/LZO/NiW samples annealed in oxidation atmosphere with different oxygen partial pressures less than 20%, respectively. The initial (0 0 *l*) textured peak intensity of buffer layers gradually decreases and the textured peaks finally disappear. The disappearance of LZO (0 0 4) peaks is accompanied by the emergence of the oxides phases related to Ni and W in LZO/NiW when oxygen partial pressure reaches 20% in annealing process. Different from this process, there seems to be a transition stage with the formation of microcrystal, where no any obvious reflections peaks in XRD spectrums are detected for CeO_2/NiW and CeO_2/LZO/NiW annealed in oxidation atmospheres with 2% and 10% oxygen partial pressures. Moreover, the oxide phases of Ni and W cannot be observed in LZO/NiW, CeO_2/NiW and CeO_2/LZO/NiW until the oxygen amount in annealing atmosphere exceeds 10%, which is called their critical oxygen partial pressure. This point illuminates that the barrier against oxygen diffusion for LZO is better than that for CeO_2 with the same film thickness. Fig. 4(d), which represents the intensity ratio computed through dividing the intensity of (0 0 *l*) peaks of the buffer layers by that of NiW (0 0 2) from XRD patterns obtained for above-mentioned samples with three different buffer layer architectures annealed in oxidation atmosphere, shows that, the intensity ratio of textured peaks of the buffer layers, which gives an estimate of oriented single-crystalline fraction in the films, decreases with the increase of oxygen partial pressure in annealing atmosphere. In this process, the slowest decreasing speed is observed for the relative intensity of LZO (0 0 4) peak, while the

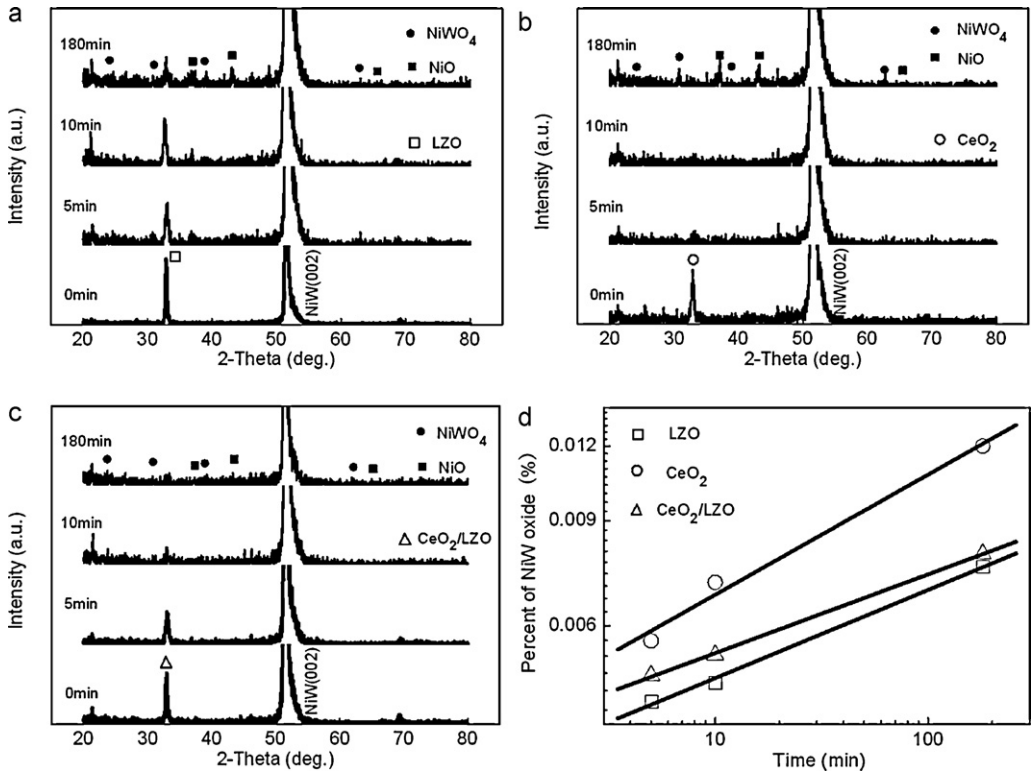

Fig. 5. Typical $\theta - 2\theta$ XRD pattern for as-grown and annealed (a) LZO/NiW, (b) CeO_2/NiW and (c) CeO_2/LZO/NiW samples for different dwelling time, respectively; (d) the percentage of NiW oxides in three kinds of samples as a function of dwelling time.

reducing rate of the intensity ratio of CeO_2 (0 0 2) peak is rapidest. Possible reason for the influence of oxygen partial pressure on the oxygen diffusion is that the nucleation process of oxides related to NiW is controlled by their activation energy, which should decrease with the increase of the oxygen partial pressure [24] and their activation energy may relate to the intrinsic oxygen diffusion coefficient of the buffer layers. Therefore, it can be considered that the decreasing rate of the intensity ratio for textured peaks of the buffer layer may be accelerated with the increase of the intrinsic oxygen diffusion coefficient of the buffer layer.

Next, the influence of dwelling time on oxygen diffusion in the buffer layers at their critical temperature and critical oxygen partial pressure in annealing processes is studied and then the kinetics of oxygen diffusion would be explored. Fig. 5(a)–(c) shows typical $\theta - 2\theta$ XRD patterns for the above-mentioned samples with three kinds of different textured buffer layers annealed for different dwelling time in Ar–10%O_2. The intensity of LZO (0 0 4) peak decreases slowly as the dwelling time prolongs in annealing process and the LZO (0 0 4) peak even coexists with the oxides reflections peaks related to Ni and W after the dwelling time is prolonged to 180 min. On the contrary, the intensity of CeO_2 (0 0 2) textured peaks rapidly decrease and suddenly disappear, while the oxides phases of NiW substrate are observed in CeO_2/NiW even annealed for a short dwelling time in Ar–10%O_2. Fig. 5(d) shows the percentage of oxides related to Ni and W (wt%) as a function of the dwelling time in the Ar–10%O_2 at a logarithmic scale. The amount of oxides related to Ni and W quickly increases in CeO_2/NiW as the annealing time prolongs, while this process is relatively slow in LZO/NiW and CeO_2/LZO/NiW. At the same time, the percentage of these oxides in CeO_2/NiW is much greater than that in other samples under the same annealing condition. The kinetics of this oxidation process can be described by Rönnquist equation as follows [23],

$$\mathrm{Lg}\Delta m = \frac{1}{n}(\mathrm{Lg}\,k + \mathrm{Lg}\,t) \tag{4}$$

where Δm is the amount of oxide formed at dwelling time t and the exponent n varies with temperature, k denotes the reaction rate constant. For each samples with a fixed buffer layer architecture, k is a constant at a fixed temperature, so a linear relationship is expected between the Δm and t at a logarithmic scale.

In addition, it can be considered that Δm is proportional to the percentage of NiW oxides (wt%) for the same dwelling time in annealing process. This is given by expression (5):

$$\Delta m \propto \mathrm{wt\%} \tag{5}$$

According to Eq. (4) and expression (5), it can be derived as:

$$\mathrm{Lg\ wt\%} = \frac{1}{n}(\mathrm{Lg}\,k + \mathrm{Lg}\,t) + c \tag{6}$$

where c denotes a constant in each samples with the same buffer layer architecture.

The percentage of oxides related to Ni and W increases linearly with the increase of dwelling time in the annealing process at logarithmic scale. It can be seen that the slopes of the lines among these samples with different buffer layer architecture are rather different. The n value is smallest for CeO_2/NiW, while it is very close to each other for LZO/NiW and CeO_2/LZO/NiW. Correspondingly, the oxidation of NiW in CeO_2/NiW is much easier than that in other two kinds of the samples at their critical temperature. It can be also explained by the direct influence of intrinsic oxygen diffusion coefficient of the buffer layers on the reaction rate constant k and the exponent n of the oxidation reaction of NiW substrate at the fixed annealing temperature.

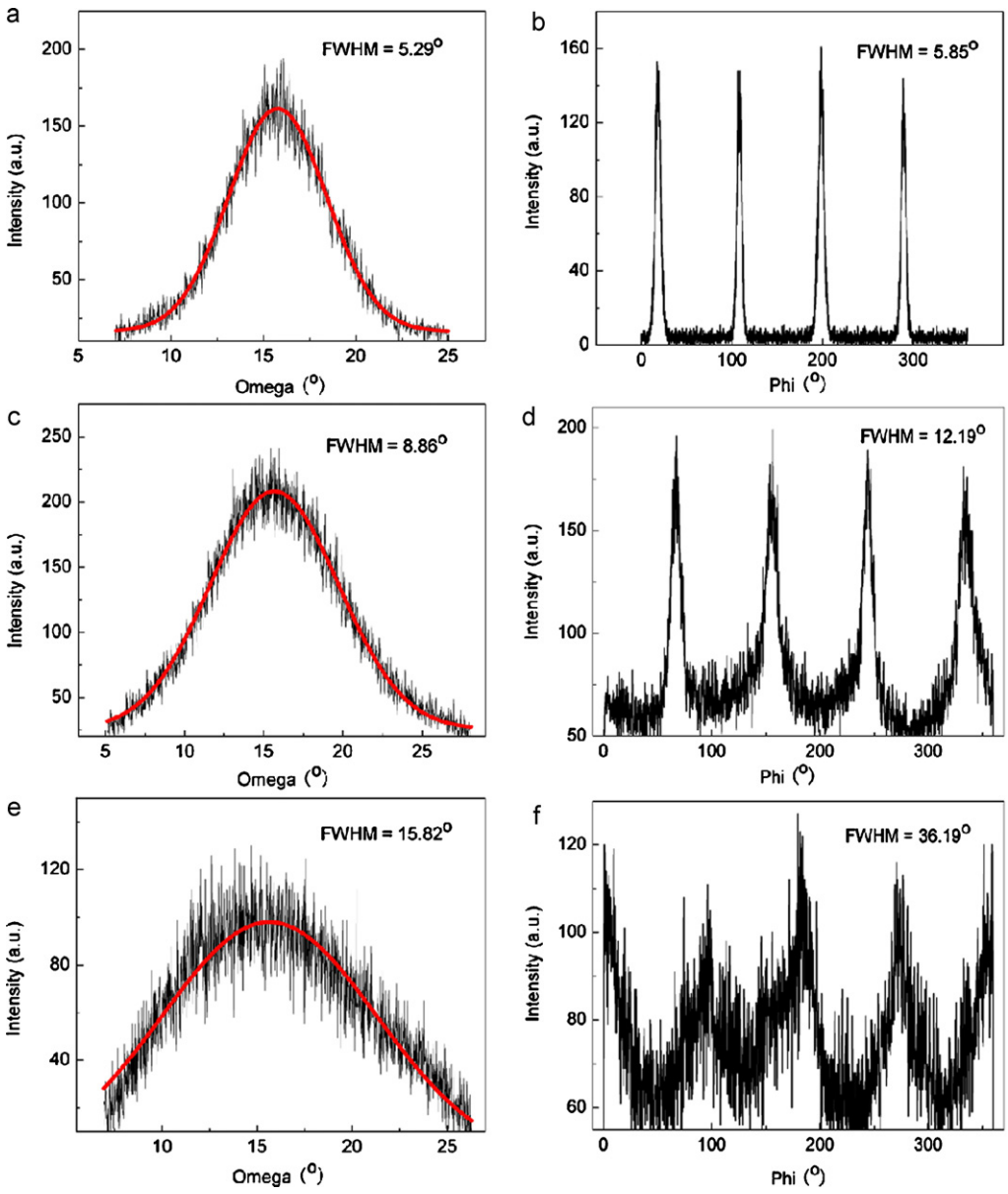

Fig. 6. Out-of-plane and in-plane scans of LZO buffer layers with and without annealing in oxidation atmosphere.

The omega (out-of-plane) and phi (in-plane) scans of the LZO buffer layers on Ni–W substrates with and without annealing in oxidation atmosphere are shown in Fig. 6. The LZO buffer layer crystallized in Ar–4%H_2 shows a very good textured degree, with the FWHM values obtained from omega and phi scans of 5.29° and 5.85° as shown in Fig. 6(a) and (b), which are very close to that reported by IFW [9]. However, the FWHM values of LZO (0 0 4) and LZO (2 2 2) drastically increase when the LZO/NiW was annealed in oxidation atmosphere. For LZO/NiW annealed in Ar–10%O_2 at 750 °C for 10 min, the FWHM values are 8.86° and 12.19°, while that of the LZO buffer layer is 15.82° and 36.19° when the LZO/NiW was annealed in air at 800 °C for 10 min. It indicates that the oxidation of NiW substrate results in the obvious decrease of the degree of texture for LZO buffer layer. Moreover, it should be pointed out that the increase of in-plane alignment of LZO buffer layer is more rapid than that of its out-of-plane alignment during the annealing process in oxidation atmosphere, which is related to the growth mode of the oxides related to NiW substrate.

Fig. 7 shows the AFM images for the as-grown and annealed LZO/YSZ samples in oxidation atmosphere. Fig. 7(a) represents the surface topology of LZO processed in Ar–4%H_2. The round-shape grains have an average grain size of about 30 nm and the root means square roughness value (Rrms) of 0.53 nm is calculated over an area of 1 μm^2, which indicates a very smooth LZO surface on YSZ (0 0 *l*) single crystal substrate. Fig. 7(b)–(d) shows the morphology of LZO films annealed in Ar–0.5% O_2, Ar–10% O_2 and pure oxygen, respectively. The surface roughness slightly increases and then remains constant with the increase of oxygen partial pressure in annealing atmosphere. The observed typical values increase from 0.98 nm in Ar–0.5% O_2 to 1.48 nm in Ar–10% O_2, and finally to 1.40 nm in pure oxygen. The LZO samples annealed in the annealing atmosphere with low oxygen partial pressure show the similar surface morphology with that of as-grown LZO/YSZ, whereas the sample annealed in pure oxygen indicates a volcanic-vent shaped surface structure although no effect of metal atom diffusion from the substrate is taken into account. This suggests that the surface mor-

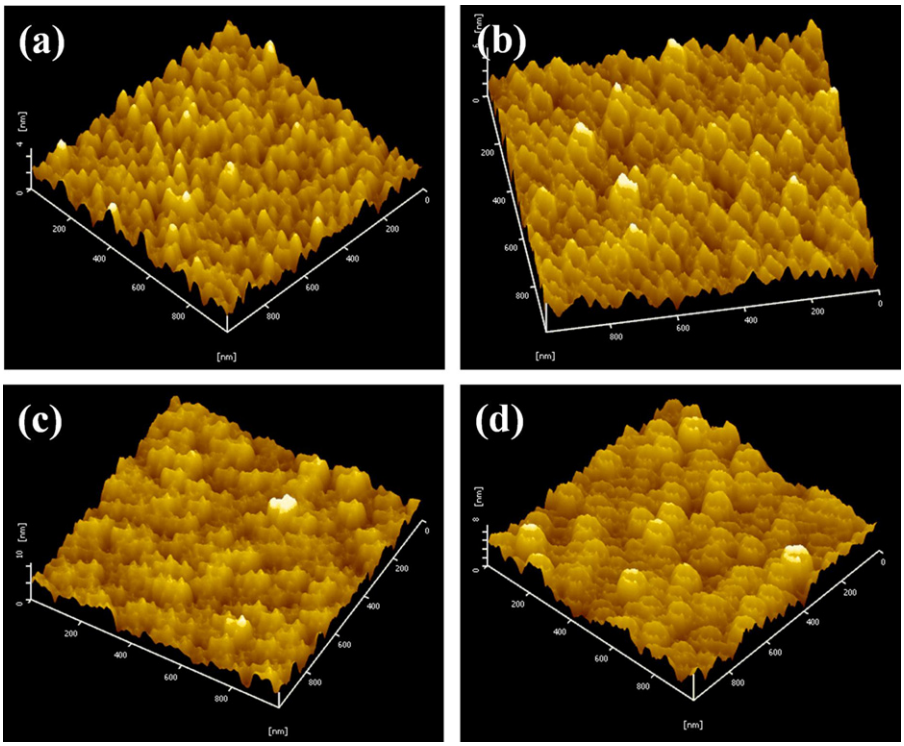

Fig. 7. AFM images for (a) as-grown and annealed LZO/YSZ samples in (b) Ar–0.5% O_2, (c) Ar–10% O_2 and (d) O_2, respectively.

phology evolution is related to the change of the oxygen vacancy concentration in the LZO films which underwent the annealing in oxygen.

A cross-section of the LZO buffer layer on Ni–W substrate is shown in Fig. 8 and a very sharp interface of the LZO buffer layer and Ni–W substrate could be seen. The LZO buffer layer appeared homogeneous in thickness and without obvious macroscopic defects. The thickness of LZO buffer layer was determined to be around 70 nm.

Figs. 9, 10 and 11 show the SEM images of above-mentioned as-grown and annealed samples with different buffer layer architectures at their critical temperatures for 10 min in oxidization atmosphere with different oxygen partial pressures, respectively. For as-grown samples, we hardly find any surface defect at current observation scope, implying a very good epitaxial growth of these buffers on NiW substrates. After annealing in pure argon, the surfaces of all samples are still smooth, continuous as well as crack-free and the NiW grain-boundary grooves are found to be completely covered. For LZO/NiW annealed in argon, there is no significant difference in the surface morphology compared with that of the as-prepared sample, suggesting a good stability of the surface. For CeO_2/NiW and CeO_2/LZO/NiW, we observe no clear contour of the grains in the top layer of CeO_2, although it seems that there exists slight growing-up of the CeO_2 grains. This basically agrees with the suppressed intensity of the textured peaks and no obvious diffraction peaks of the Ni/W oxides investigated by XRD as shown in Fig. 4. As the oxygen partial pressure in annealing atmosphere increases to 2%, several large grains are observed on the surface of LZO/NiW. For CeO_2/NiW, the CeO_2 grains seem to become obscurer. The CeO_2/LZO/NiW sample hence shows a combined surface characteristic as shown in Fig. 11(d). The significant change of the surface grain morphology in fact reflects the oxidation process when the oxygen partial pressure in annealing atmosphere reaches 2%. With the increase of oxygen partial pressure up to 10% the surface morphology of all samples is completely different from that of as-grown samples. The oxide grain accumulations with an average size of 1 μm, which are supposed to be plate-like NiO and fine-grain $NiWO_4$ judged by XRD patterns and EDS data, are detected on the surface of LZO/NiW. For CeO_2/NiW, a higher density of the blurred grains are observed on the sample surface and this is in agreement with fully suppression of the diffraction peaks of possible crystallized phases as shown in Fig. 4. When three kinds of the samples were annealed in air, the crystallized oxide phases related to Ni and W begin to be detectable. The LZO/NiW sample shows a morphology superposition of small and large islands. Based on the measured XRD and EDS data, we believe that the small and large size islands may be $NiWO_4$ and NiO, respectively. For CeO_2/NiW, many uniformly distributed square grains with a diameter of about 200 nm are observed, where some cracks appear along the grain-boundaries of NiW substrate. The XRD spectrum of this sample also suggests that the diffraction peaks of NiO are heavily suppressed and therefore these square grains should be $NiWO_4$. For CeO_2/LZO/NiW, a

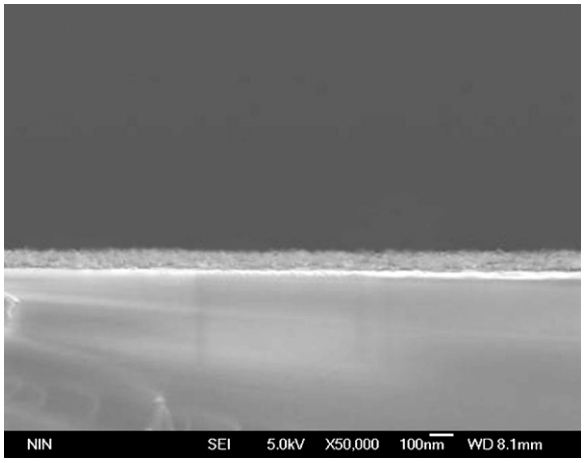

Fig. 8. Cross-section of LZO buffer layer on Ni–W substrate.

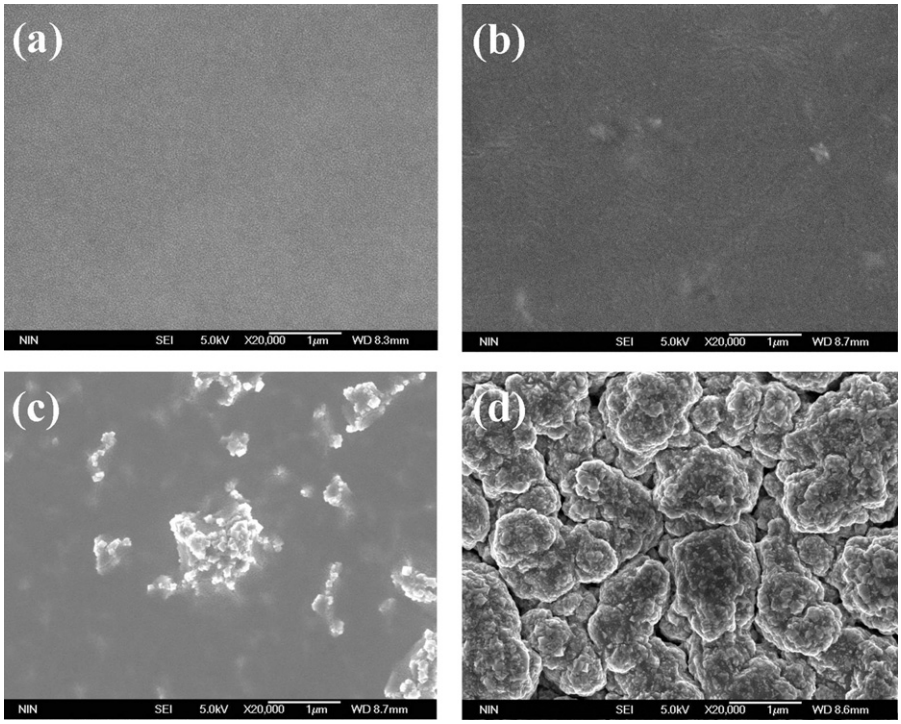

Fig. 9. SEM micrographs of the annealed LZO/NiW samples in (a) Ar, (b) Ar–2% O_2, (c) Ar–10% O_2 and (d) air, respectively.

mixed grain morphology could be expected as shown in Fig. 11(d). Here it should be pointed out that the formation of some micro-crystal grains detected by SEM for CeO_2/NiW annealed in Ar–2% O_2 and Ar–10% O_2 agrees well with the suppression of all of diffraction peaks (see Fig. 4(b)). It is likely because that the morphology evolution of these samples is related to the nucleation energy of relevant oxides influenced by the oxygen partial pressure in annealing atmosphere.

Figs. 12–14 show the surface morphologies of the as-grown and annealed LZO/NiW, CeO_2/NiW and CeO_2/LZO/NiW samples at their critical temperatures in Ar–10%O_2 for different dwelling time, respectively. A few needle-like grains appear on the LZO/NiW surface annealed at 750 °C in Ar–10%O_2 for 5 min. Then some large grains, which are presumably the oxides of Ni and W, are observed after LZO/NiW annealing for 10 min. As the annealing time prolongs to180 min, the LZO/NiW surface is locally covered by the oxide

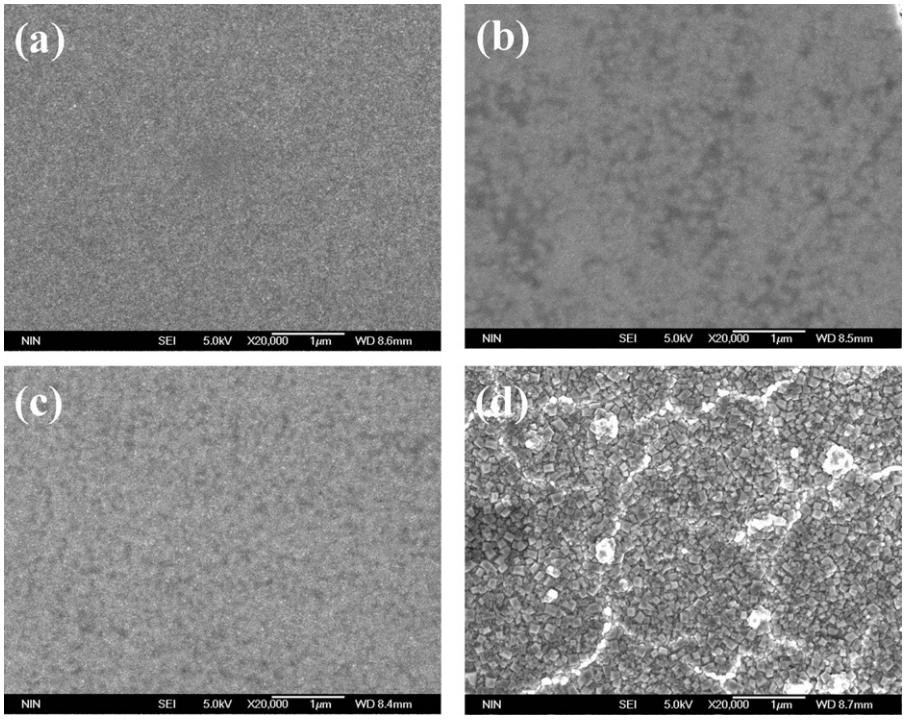

Fig. 10. SEM images of the annealed CeO_2/NiW samples in (a) Ar, (b) Ar–2% O_2, (c) Ar–10% O_2 and (d) air, respectively.

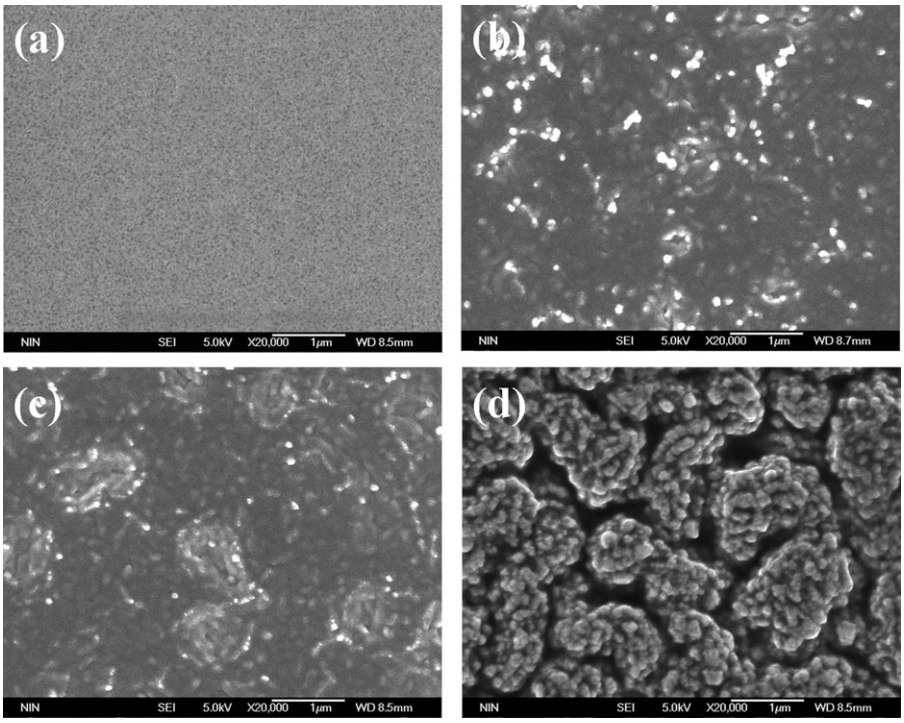

Fig. 11. SEM micrographs of the annealed CeO_2/LZO/NiW samples in (a) Ar, (b) Ar–2% O_2, (c) Ar–10% O_2 and (d) air, respectively.

grains with a 200-nm size. This means that the long time annealing in oxidation atmosphere leads to de-wetting for LZO/NiW. For the CeO_2/NiW annealed at 550 °C in Ar–10% O_2 for less than 10 min, we did not detect the abrupt change of the grain size on their surface morphology compared to the as-grown sample. However, the formation micrograin together with strong suppression of the diffraction peaks is still observed as shown in Figs. 5 and 13. The surface of the CeO_2/NiW sample annealed for 180 min is covered completely by the quadrate oxide grains of Ni and W. At the same time, some cracks, which are just located at the NiW grain-boundary grooves, appear on the surface of CeO_2/NiW. Some bulges are observed on the surface of CeO_2/LZO/NiW annealed for 5 min, then these bulges become further salient and their amount increases as the dwelling time prolongs to 10 min. Until the annealing time is extended to180 min, the entire surface of sample is not covered by quadrate grains yet. The transformation of the surface

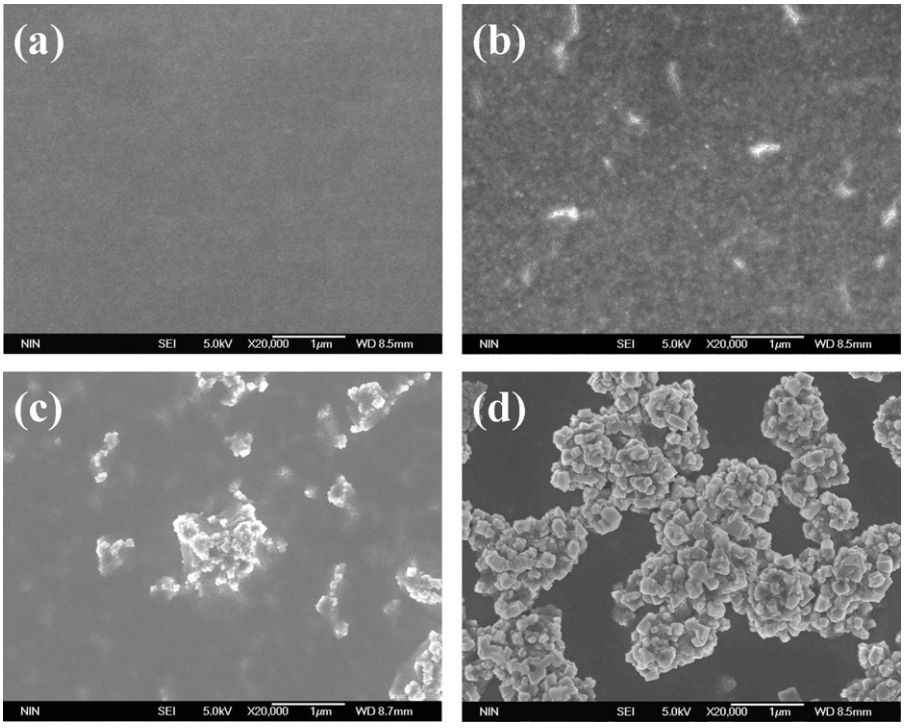

Fig. 12. SEM images of the annealed LZO/NiW samples in oxidation atmosphere for (a) 0 min, (b) 5 min, (c) 10 min and (d) 180 min, respectively.

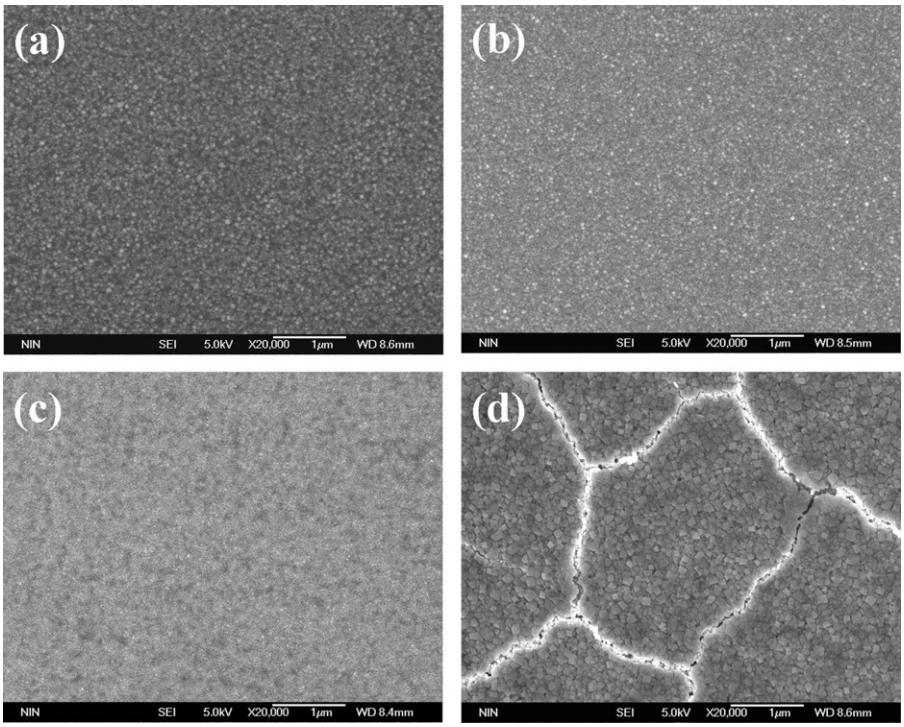

Fig. 13. SEM micrographs of the annealed CeO_2/NiW samples in oxidation atmosphere for (a) 0 min, (b) 5 min, (c) 10 min and (d) 180 min, respectively.

morphology of these samples may be attributed to the influence of the difference between oxygen diffusion behavior for LZO or CeO_2 as the buffer layer on the nucleation process of oxides related to the NiW substrate. Combined the SEM and XRD data, we suggest that the formation of the oxides related to Ni and W with no any crystalline orientation could not destroy completely the original texture of LZO buffer layers if the oxygen partial pressure in annealing atmosphere is not too high.

$NiWO_4$ and NiO layers between buffer and substrate could easily form if the YBCO layer underwent a heat treatment with a long duration at high temperature during preparation of the YBCO superconducting layer by TFA-MOD method even if the oxygen partial pressure was only Ar–0.1% O_2. These $NiWO_4$ and NiO layers consist of many small crystals with random orientations [15]. Therefore, we could suppose that there exist these kinds of oxide layers in the CeO_2/NiW and CeO_2/LZO/NiW samples annealed in

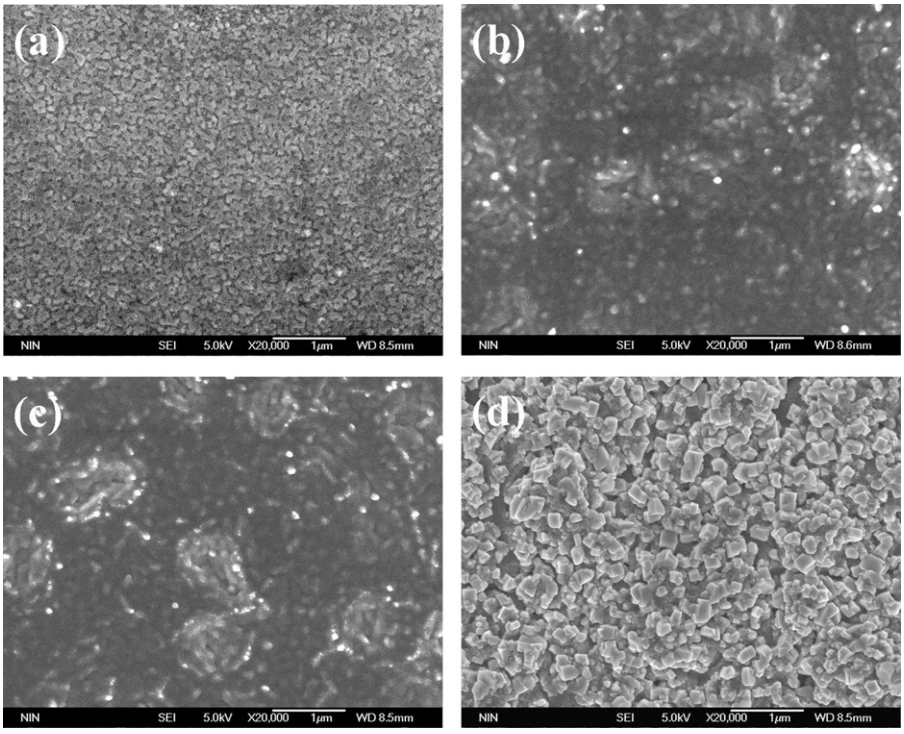

Fig. 14. SEM images of the annealed CeO_2/LZO/NiW samples in oxidation atmosphere for (a) 0 min, (b) 5 min, (c) 10 min and (d) 180 min, respectively.

oxidation atmosphere. When these oxide layers reach to a certain thickness, they could be detected on the sample surface and the texture of the buffer layers may be completely destroyed. According to the Wagner theory, the driving force that govern the formation of oxide films related to Ni(W) is determined by the Gibbs free energy change of the oxidation reaction between metal and oxygen atoms and the concentration gradient of related ingredients in the oxides layers. Although the Gibbs free energy change about the formation of $NiWO_4$ is smaller than that of NiO, the amount of NiO is still larger than that of $NiWO_4$ in above-mentioned samples annealed in oxidation atmosphere due to a greater supply amount of Ni than W in the substrate.

Now we consider different influence of oxygen diffusion coefficient of buffer layer materials on oxygen atom diffuse and subsequent oxidation reaction. Because the intrinsic oxygen diffusion coefficient of CeO_2 is much larger than that of $La_2Zr_2O_7$, the oxygen diffusion through the crystal lattices is predominant in CeO_2 buffer, whereas the oxygen diffusion through pores plays a leading role in $La_2Zr_2O_7$ buffer. Thus a slow oxygen diffusion rate and a small nucleation density of oxides related to NiW substrate result in a slow reduction of the LZO (0 0 *l*) textured peaks with the increase of oxygen partial pressure and the prolongation of dwelling time in annealing profile and also the appearance of sporadically distributed oxides related to Ni and W on the surface of LZO/NiW samples annealed in a low oxygen partial pressure for short dwelling time in annealing process. Eventually, these sporadically distributed oxides grow up to form the plenty of oxide islands with a large size on the surface of LZO/NiW samples annealed in air for a short time or in Ar–10%O_2 for a long dwelling time. The LZO (0 0 4) peak could still be detected in LZO/NiW annealed in Ar–10% O_2 for 180 min together with the appearance of the oxide phases related to Ni and W. It indicates that the local oxidation of the substrate could not disturb completely the texture of the buffer layers. The fact that the coverage of NiW oxides on the surface of LZO/NiW annealed in air for 10 min is larger than that annealed in Ar–10%O_2 for 180 min may be explained by a larger initial nucleation rate of oxides related to NiW substrate in the former process than that of the later. However, the structure and texture of the buffer layers were quickly disturbed in CeO_2/NiW even annealed in oxidation atmosphere with a low oxygen partial pressure for a short dwelling time due to the rapid oxidation of the substrate, finally these oxide grains with a uniform size were observed on the surface of the samples with the increase of thickness of oxide film related to Ni and W. Besides, some cracks formed on the surface of CeO_2/NiW samples annealed in air for a short time or in Ar–10% O_2 for a long dwelling time. It implies that the defects, such as grain boundaries of the metal substrate may serve as paths for enhanced oxygen diffusion. By contrast, the total oxygen diffusion coefficient of CeO_2/LZO is between that of LZO and CeO_2.

The behavior of oxygen diffusion for buffer layers in coated conductors, resulting in the formation of unwanted oxides and even destruction of the texture of buffers, is involved in a rather complicated process. The oxidation reaction can occur only if the oxygen atoms from heat treatment atmosphere and metal atoms from NiW substrates diffuse through continuous buffer layers and finally react with each other. Usually, the (0 0 1) crystal plane of fcc metals can be oxidized more rapidly than the (1 1 0) and (1 1 1) planes, and the oxygen diffusion coefficient of buffer layers is frequently a crucial effect to the oxidation rate of NiW substrate [24]. The variation of texture and morphology of buffer layers is affected by the change of the oxide layers about the NiW substrate which is related to the temperature, oxygen partial pressure and dwelling time in annealing process. The formation of oxides about metal substrate takes place by the mechanism involving nucleation and growth of these oxides. The nucleation of oxides about the NiW substrate may occur at the interface between buffer layers and the metal substrate due to a lower interfacial energy. With rising the annealing temperature, the migration of metal and oxygen atoms and the growth of oxide layers related to NiW substrate will be enhanced. During a short period of time the nucleation density of the oxides related to NiW substrate increases significantly with the increase of oxygen partial pressure in annealing atmosphere, the development of these oxide grains finally leads to their emergence on the sample surface. However, when the oxygen partial pressure is fixed, the nucleation density of oxides related to Ni and W can be considered as a constant in the sample. Then these oxide grains grow up from the initial nucleation centers, resulting in the formation of larger oxide grains with prolonging the dwelling time. It can be considered that the dwelling time shows less effect on the oxidation rate of NiW substrate and the destruction of buffer layer texture than the oxygen partial pressure. In conclusion, the intrinsic oxygen diffusion coefficient of buffer layer is the crucial factor of influencing the oxidation reaction of the metal substrate in the whole oxidation process other than some controllable factors including temperature, oxygen partial pressure and dwelling time in annealing process. It would decide the destruction degree of the texture and structure of buffer layer through influencing the thickness of oxide layers about metal substrate and the coverage of NiW oxides on the surface of the samples if the difference of metal diffusion degree in each buffer layers is essentially negligible.

4. Conclusions

We have systematically studied the possible diffusion barrier mechanism of coated conductors by investigating the effect of annealing in different oxygen partial pressures on the structure and morphology of the buffer layers. In addition, the behavior of oxygen diffusion of three kinds of buffer layer architectures with the same thickness on NiW substrates prepared by MOD method has been investigated by analyzing the differences of texture and morphology between the as-prepared sample and annealed samples under the different annealing temperatures, oxygen partial pressure and dwelling time conditions. Annealing in oxygen of LZO crystallized films on YSZ (0 0 *l*) single crystal substrates affects not only the lattice parameter and the crystalline degree but also the film microstructure due to the decreased oxygen vacancies in LZO pyrochlore structure. Our results show that the percentage of oxides related to NiW-substrate exponentially increases with the annealing temperature, and linearly increases with the dwelling time at logarithmic scale, while the intensity ratio of the buffer layer texture peaks decreases with the increase of the oxygen partial pressure. It indicates that the intrinsic oxygen diffusion coefficient of the buffer layer architecture directly influences the activation energy and the reaction rate of oxidation of NiW substrate, and finally affects the declining rate of buffer layer texture. Besides choosing the oxide materials with a low oxygen diffusion coefficient as buffer layers in coated conductors, adopting lower temperature, lower oxygen partial pressure and shorter dwelling time in annealing process is very important to stabilize the textured buffer structure.

Acknowledgements

This work was financially supported by the National Science Fund Program and National 863 Program of China (Grant Nos. 50872115 and 2008AA03Z202).

References

[1] Y. Matsuoka, E. Ban, H. Ogawa, K. Kurosawa, J. Alloys Compd. 239 (1996) 55–62.
[2] A.H. Robert, K.C. David, Physica C 445–448 (2006) 488–495.

[3] S.H. Wee, A. Goyal, H. Hsu, J. Li, L. Heatherly, K. Kim, T. Aytug, S. Sathyamurthy, M.P. Paranthaman, J. Am. Ceram. Soc. 90 (2007) 3529–3535.
[4] L. Arda, S. Ataoglu, J. Alloys Compd. 471 (2009) 282–290.
[5] M.S. Bhuiyan, M. Paranthaman, K. Salama, Supercond. Sci. Technol. 19 (2006) R1–R21.
[6] J.C. Wang, C.H. Yang, G.D. Hu, W.B. Wu, L. Cheng, X.M. Chen, J. Alloys Compd. 494 (2010) 285–288.
[7] J.W. Seo, J. Fompeyrine, A. Guiller, G. Norga, C. Marchiori, H. Siegwart, J.P. Locquet, Appl. Phys. Lett. 83 (2003) 5211–5213.
[8] M.S. Bhuiyan, M. Paranthaman, S. Sathyamurthy, T. Aytug, S. Kang, D.F. Lee, A. Goyal, E.A. Payzant, K. Salama, Supercond. Sci. Technol. 16 (2003) 1305–1309.
[9] K. Knoth, R. Hühne, S. Oswald, L. Schultz, B. Holzapfel, Supercond. Sci. Technol. 18 (2005) 334–339.
[10] K. Knoth, R. Hühne, S. Oswald, L. Schultz, B. Holzapfel, Acta Mater. 55 (2007) 517–529.
[11] Z.M. Yu, P. Odier, L. Ortega, P.X. Zhang, C.S. Li, X.H. Liu, L. Zhou, J. Alloys Compd. 460 (2008) 519–523.
[12] K. Knoth, R. Hühne, S. Oswald, L. Molina, O. Eibl, L. Schultz, B. Holzapfel, Thin Solid Films 516 (2008) 2099–2108.
[13] T. Caroff, S. Morlens, A. Abrutis, M. Decroux, P. Chaudouët, L. Porcar, Z. Saltyte, C. Jiménez, P. Odier, F. Weiss, Supercond. Sci. Technol. 21 (2008), 075007 1–8.
[14] S. Engel, R. Hühne, K. Knoth, A. Chopra, N.H. Kumar, V.S. Sarma, P.N. Santhosh, L. Schultz, B. Holzapfel, J. Cryst. Growth 310 (2008) 4295–4300.
[15] V. Cloet, T. Thersleff, O. Stadel, S. Hoste, B. Holzapfel, I.V. Driessche, Acta Mater. 58 (2010) 1489–1494.
[16] A. Pomar, M. Coll, A. Cavallaro, J. Gàzquez, J.C. González, N. Mestres, F. Sandiumenge, T. Puig, X. Obradors, J. Mater. Res. 21 (2006) 1106–1116.
[17] Y. Miyanaga, R. Teranishi, K. Yamada, N. Mori, M. Mukaida, T. Kiss, M. Inoue, K. Nakaoka, M. Yoshizumi, T. Izumi, Y. Shiohara, M. Nanba, S. Awaji, K. Watanabe, Physica C 469 (2009) 1418–1421.
[18] R. Teranishi, J. Yoshida, N. Mori, K. Yamada, M. Mukaida, T. Kiss, M. Inoue, J. Matsuda, K. Nakaoka, T. Izumi, Y. Shiohara, Physica C 469 (2009) 1332–1335.
[19] S.H. Jang, J.H. Lim, C.M. Lee, E.C. Park, S.M. Hwang, J.H. Choi, J.H. Shim, J.H. Park, W. Kim, J. Joo, Trans. Nonferrous Met. Soc. China 19 (2009) 956–960.
[20] S. Sathyamurthy, M. Paranthaman, L. Heatherly, P.M. Martin, E.D. Specht, A. Goyal, T. Kodenkandath, X.P. Li, M.W. Rupich, J. Mater. Res. 21 (2006) 910–914.
[21] R.P. Sun, M.H. Pu, G. Li, W.T. Wang, M. Pan, H. Zhang, M. Lei, W. Wu, X. Zhang, Y. Yang, Y. Zhang, Y. Zhao, Phys. Status Solidi A 206 (2009) 1414–1419.
[22] L. Molina, K. Knoth, S. Engel, B. Holzapfel, O. Eibl, Supercond. Sci. Technol. 19 (2006) 1200–1208.
[23] K.R. Lawless, Rep. Prog. Phys. 37 (1974) 231–316.
[24] R. Herehl, N.N. Khoi, T. Homma, W.W. Smeltzer, Oxid. Met. 4 (1972) 35–49.